

On the influence of a non-cohesive fines content on small strain stiffness, modulus degradation and damping of quartz sand

T. Wichtmannⁱ⁾ M.A. Navarrete Hernándezⁱⁱ⁾ Th. Triantafyllidisⁱⁱⁱ⁾

Abstract: The influence of a non-cohesive fines content on small-strain shear modulus G_{\max} , small-strain constrained elastic modulus M_{\max} , shear modulus degradation $G(\gamma)/G_{\max}$, damping ratio $D(\gamma)$ and threshold shear strain amplitudes γ_{tl} and γ_{tv} has been studied in approx. 130 resonant column (RC) tests with additional P-wave measurements by means of piezoelectric elements. Specially mixed continuous grain size distribution curves of a quartz sand with varying fines contents ($0 \leq FC \leq 20$ %, defined as the mass percentage of grains with size $d < 0.063$ mm according to DIN standard code) and uniformity coefficients ($1.5 \leq C_u \leq 50$) have been tested at different relative densities and pressures. A significant decrease of G_{\max} and M_{\max} with increasing fines content was observed, while the modulus degradation curves $G(\gamma)/G_{\max}$ were found rather independent of FC . A pressure-dependent decrease of the damping ratio and a slight increase of the threshold shear strain amplitudes γ_{tl} and γ_{tv} with fines content were measured. Extensions of several empirical equations for G_{\max} , M_{\max} , $G(\gamma)/G_{\max}$ and $D(\gamma)$ considering the influence of the fines content are proposed in the paper.

Keywords: Small strain stiffness; Modulus degradation; Damping ratio; Quartz sand; Fines content; Resonant column tests

1 Introduction

Although measurements of the S- and P-wave velocity in situ have become a commonplace tool for the design of foundations subjected to a cyclic or dynamic loading during recent years, empirical formulas for the dynamic soil properties may be beneficial for feasibility studies and preliminary design calculations, for final design calculations in small projects or to provide an order-of-magnitude check against the in situ values (Gazetas [7]). In particular, empirical equations for the modulus degradation or the increase of damping ratio with increasing shear strain amplitude are useful since these curves are difficult to measure in situ.

The secant shear modulus G of the shear strain - shear stress hysteresis is usually described by a multiplicative approach $G = G_{\max} F(\gamma)$ with the small strain shear modulus G_{\max} and a modulus reduction factor $F(\gamma)$ depending on shear strain amplitude γ . The small strain shear modulus of non-cohesive soils is often estimated using Hardin's formula [8, 11] (given in its dimensionless form here)

$$G_{\max} = A \frac{(a - e)^2}{1 + e} \left(\frac{p}{p_{\text{atm}}} \right)^n p_{\text{atm}} \quad (1)$$

with void ratio e , mean pressure p , atmospheric pressure $p_{\text{atm}} = 100$ kPa and with the constants $A = 690$, $a = 2.17$ and $n = 0.5$ for round grains and $A = 320$, $a = 2.97$ and $n = 0.5$ for angular grains.

Unfortunately, Eq. (1) does not consider the strong influence of the grain size distribution curve on small-strain

stiffness. For constant values of void ratio and pressure, the small strain shear modulus considerably decreases with increasing uniformity coefficient $C_u = d_{60}/d_{10}$ while it is rather independent of mean grain size d_{50} (Iwasaki & Tatsuoka [12], Wichtmann & Triantafyllidis [25]). Eq. (1) with its commonly used constants may strongly over-estimate the G_{\max} -values of clean well-graded granular materials (see Figure 1). A similar reduction with increasing C_u was observed for the constrained elastic modulus $M_{\max} = \rho v_P^2$ (Wichtmann & Triantafyllidis [26]). Furthermore, for a certain shear strain amplitude modulus degradation was found larger for sands having higher C_u -values (Wichtmann & Triantafyllidis [27]). Extensions of empirical equations for G_{\max} , M_{\max} and $G(\gamma)/G_{\max}$ considering the influence of C_u have been proposed in [25-27]. These equations are summarized in Section 2.

A further significant reduction of the small strain stiffness may result from a non-cohesive fines content. It is obvious in Figure 2 which collects respective G_{\max} data from several studies in the literature (Iwasaki & Tatsuoka [12], Randolph et al. [19], Salgado et al. [21], Sahaphol & Miura [20]). On the ordinate the small-strain shear modulus G_{\max} at a certain fines content FC is divided by the value $G_{\max}(FC = 0)$ for clean sand at same values of void ratio and pressure. Based on Figure 2 the decrease of G_{\max} with FC is pressure-dependent and also influenced by the type of the two ingredients (sand and silt).

In the studies documented in the literature so far either only a low number of tests was performed or relatively coarse granular materials (medium coarse sands up to fine gravels) were mixed with fines, resulting in gap-graded mixtures. However, most real soils with fines are not gap-graded but have a rather continuous grain size distribution curve. Furthermore, no data on the influence of the fines content on constrained elastic modulus M_{\max} , Poisson's ratio ν ,

ⁱ⁾Researcher, Institute of Soil Mechanics and Rock Mechanics, Karlsruhe Institute of Technology, Germany (corresponding author). Email: torsten.wichtmann@kit.edu

ⁱⁱ⁾Consultant Engineer, ITASCA, Dr. José Luis Aguilar 1178, Providencia, 7501360 Santiago (Chile)

ⁱⁱⁱ⁾Professor and Director of the Institute of Soil Mechanics and Rock Mechanics, Karlsruhe Institute of Technology, Germany

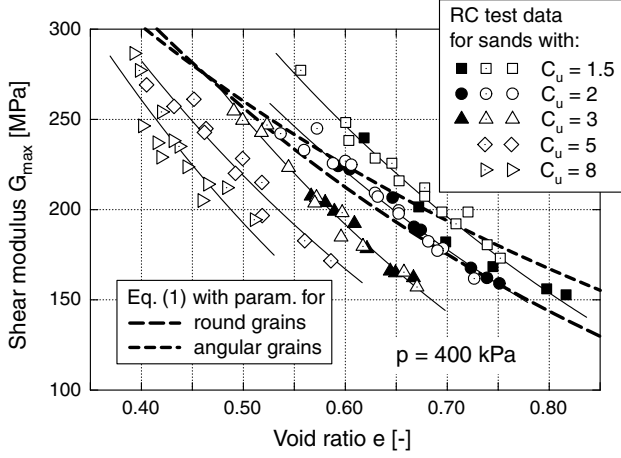


Fig. 1: Decrease of small strain shear modulus G_{\max} with increasing uniformity coefficient C_u , figure adapted from [25]

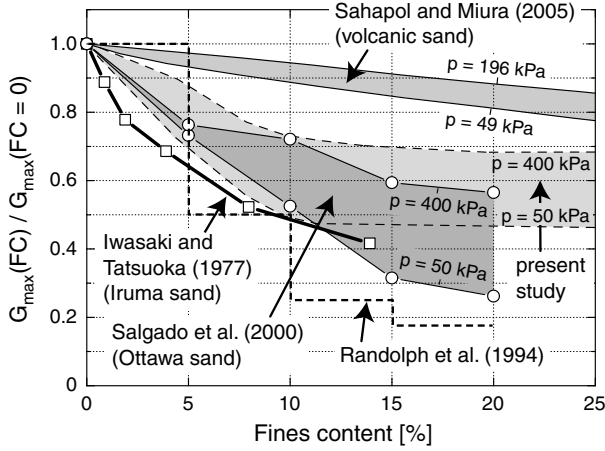


Fig. 2: Reduction of G_{\max} with increasing content of non-cohesive fines, comparison of different studies in the literature

modulus degradation curves $G(\gamma)/G_{\max}$ or damping ratio curves $D(\gamma)$ are available in the literature. Therefore, in order to extend the C_u -dependent empirical equations developed for clean sands (Section 2) by the influence of a fines content, approx. 130 resonant column (RC) tests with additional P-wave measurements have been performed on several silty sands having varying FC - and C_u -values. This paper presents the test results and reports on the extensions of the various empirical formulas by the influence of a fines content.

2 Extended empirical formulas for clean sands

For clean sands, in order to consider the reduction of G_{\max} with C_u , the following correlations of the parameters A , a and n of Eq. (1) with C_u have been proposed in [25]:

$$A = 1563 + 3.13 C_u^{2.98} \quad (2)$$

$$a = 1.94 \exp(-0.066 C_u) \quad (3)$$

$$n = 0.40 C_u^{0.18} \quad (4)$$

Note, that although the factor A increases with C_u according to Eq. (2), the combination with Eqs. (3) and (4), describing a decrease of a and an increase of n with C_u , predicts a decreasing small-strain shear modulus with

increasing uniformity coefficient. The correlations (2) to (4) are based on more than 160 resonant column (RC) tests on 25 different grain size distribution curves with linear shape in the semi-logarithmic scale. Eqs. (2) to (4) have been confirmed for mean grain sizes in the range $0.1 \leq d_{50} \leq 6$ mm and for uniformity coefficients in the range $1.5 \leq C_u \leq 15$. A correlation of G_{\max} with relative density $D_r = (e_{\max} - e)/(e_{\max} - e_{\min})$ is less accurate than the empirical equations formulated in terms of void ratio, but may suffice for practical purposes [25]:

$$G_{\max} = 74000 \frac{1 + D_r[\%]/100}{(11.6 - D_r[\%]/100)^2} \left(\frac{p}{p_{\text{atm}}} \right)^{0.48} p_{\text{atm}} \quad (5)$$

Based on measurements of the P-wave-velocity v_P , a set of equations similar to (1) to (4) has been developed for the small-strain constrained elastic modulus M_{\max} of clean sands (Wichtmann & Triantafyllidis [26]):

$$M_{\max} = A \frac{(a - e)^2}{1 + e} \left(\frac{p}{p_{\text{atm}}} \right)^n p_{\text{atm}} \quad \text{with} \quad (6)$$

$$A = 3655 + 26.7 C_u^{2.42} \quad (7)$$

$$a = 2.16 \exp(-0.055 C_u) \quad (8)$$

$$n = 0.344 C_u^{0.126} \quad (9)$$

The correlation between M_{\max} and D_r reads:

$$M_{\max} = 2316 \left(1 + 1.07 \frac{D_r[\%]}{100} \right) \left(\frac{p}{p_{\text{atm}}} \right)^{0.39} p_{\text{atm}} \quad (10)$$

Several empirical equations for the modulus degradation curves $G(\gamma)/G_{\max}$ have been extended by Wichtmann & Triantafyllidis [27] in order to consider the C_u -dependence. Amongst others, the parameter a of the equation proposed by Hardin & Drnevich [9]

$$F(\gamma) = \frac{G(\gamma)}{G_{\max}} = \frac{1}{1 + \frac{\gamma}{\gamma_r} \left[1 + a \exp\left(-b \frac{\gamma}{\gamma_r}\right) \right]} \quad (11)$$

has been correlated with C_u :

$$a = 1.070 \ln(C_u) \quad (12)$$

In Eq. (11) $\gamma_r = \tau_{\max}/G_{\max}$ is a reference shear strain [27] and the parameter b can be set to 1.0 (Hardin & Kalinski [10]). The following simple equation is suitable as well [27]:

$$\frac{G}{G_{\max}} = \frac{1}{1 + a \gamma/\gamma_r} \quad \text{with} \quad (13)$$

$$a = 1 + 0.847 \ln(C_u) \quad (14)$$

If Eqs. (11) and (13) are applied with a reference quantity $\sqrt{p/p_{\text{atm}}}$ instead of γ_r (Hardin & Kalinski [10]), their parameters a can be estimated from the same correlation [27]:

$$a = 1093.7 + 1955.3 \ln(C_u). \quad (15)$$

Stokoe's equation [22]

$$\frac{G}{G_{\max}} = \frac{1}{1 + (\gamma/\gamma_r)^\alpha} \quad \text{with} \quad (16)$$

$$\gamma_r = \gamma \left(\frac{G}{G_{\max}} = 0.5 \right) = \gamma_{r1} \left(\frac{p}{p_{\text{atm}}} \right)^k \quad (17)$$

can be applied with $\alpha = 1.03$, $k = 0.4$ and [27]

$$\gamma_{r1} = 6.52 \cdot 10^{-4} \exp[-0.59 \ln(C_u)] \quad (18)$$

For a discussion of various empirical equations for damping ratio the interested reader is referred to [27].

Wichtmann & Triantafyllidis [25,27] have demonstrated that the extended empirical equations presented in this section are suitable to reproduce a large number of experimental data for various sands collected from the literature. Furthermore, it has been shown [28,29] that the extended empirical formulas work well also for stepwise-linear, gap-graded, S-shaped and other smoothly shaped grain size distribution curves.

3 Tested materials, test device and testing procedure

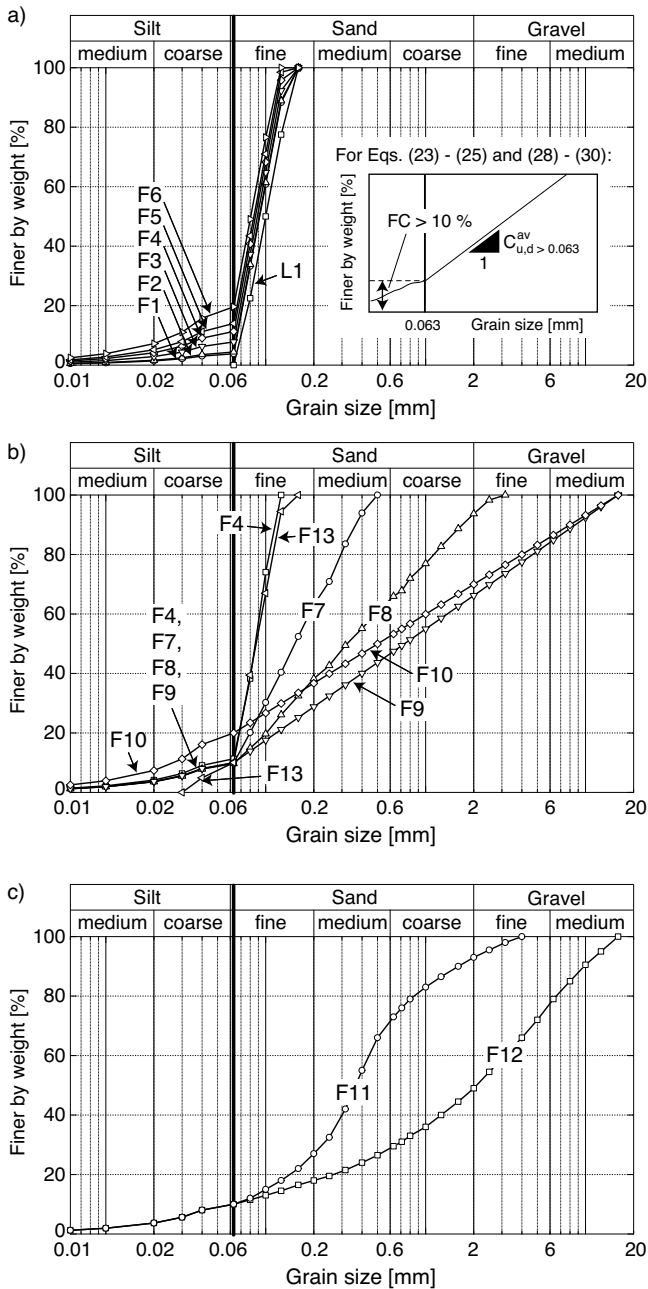


Fig. 3: Tested grain size distribution curves

The present study was performed with a natural quartz sand obtained from a sand pit near Dorsten, Germany. The grain shape is sub-angular and the specific weight is $\rho_s = 2.65 \text{ g/cm}^3$. The raw material was first sieved into 25 gradations with grain sizes between 0.063 and 16 mm. Next, grain size distribution curves with specific values of fines content FC , mean grain size d_{50} and uniformity coefficient $C_u = d_{60}/d_{10}$ have been mixed (see Figure 3). Note, that in the present study the fines content FC is defined as the mass percentage of grains with size smaller than 0.063 mm, according to German standard code DIN 18196 [2]. In many other studies in international literature, the grain size separating the fine from the coarse grains is chosen as $d = 0.074 \text{ mm}$. A further discussion of the effect of these differences in the definition of fines content is provided in Section 4.2. When mixing the sand, a quartz powder was used for the grains smaller than 0.063 mm. Table 1 summarizes the characteristics of the grain size distribution curves (d_{50} , C_u , FC) and the minimum and maximum void ratios e_{\min} and e_{\max} of the tested sands determined according to DIN 18126 [1].

The six fine sands F1 to F6 (Figure 3a) have different fines contents in the range $3.8 \% \leq FC \leq 19.6 \%$. For grain sizes $d \geq 0.063 \text{ mm}$, the grain size distribution curves of F1 to F6 are linear in the semi-logarithmic scale and parallel to each other. Furthermore, they have the same inclination as the grain size distribution curves of the clean sands or gravels L1 - L8 on which the d_{50} -influence has been studied in [25]. The shape of the grain size distribution curves for $d < 0.063 \text{ mm}$ is given by the gradation of the quartz powder. The sands F1 to F3 with $FC \leq 10 \%$ have a uniformity coefficient $C_u = 1.5$. For sands F4 to F6, the fines content $FC > 10 \%$ results in lower d_{10} -values and thus $C_u > 1.5$.

In order to study the influence of the fines content for more well-graded sands or sand-gravel mixtures, the materials F7 to F10 were mixed (Figure 3b) having 10 or 20 % fines. Their grain size distribution curves are linear at $d \geq 0.063 \text{ mm}$. In contrast, the two materials F11 and F12 (Figure 3c) have S-shaped gradations in the range $d \geq 0.063 \text{ mm}$.

The influence of the shape of the grain size distribution curve in the range $d < 0.063 \text{ mm}$ was studied on sand F13. It has $FC \approx 10 \%$ but in contrast to all other materials the fine particles contain only grains in the range $0.04 \leq d \leq 0.063 \text{ mm}$.

The resonant column (RC) device used for the present study is shown in Fig. 4. It is of the “free - free” type, meaning both the top and the base mass are freely rotatable. The prismatic top mass is equipped with two electrodynamic exciters each accelerating a small mass. This acceleration and the resulting acceleration of the top mass are measured with acceleration transducers. From these signals the torsional moment $M(t)$ and the angle of twist $\theta(t)$ at the top of the sample can be calculated. The sample is enclosed in a pressure cell. The state of stress is almost isotropic. A small stress anisotropy results from the weight of the top mass ($m \approx 9 \text{ kg}$), such that the vertical stress σ_1 is slightly higher than the lateral one σ_3 . However, for higher cell pressures this anisotropy is of secondary importance. Furthermore, test results of Yu & Richart [31] reveal that a stress anisotropy becomes significant only near failure.

A sinusoidal electrical signal is generated by a function

Sand	FC [%]	d_{50} [mm]	C_u [-]	e_{\min} [-]	e_{\max} [-]
F1	3.8	0.093	1.5	0.690	1.108
F2	4.4	0.092	1.5	0.734	1.107
F3	7.8	0.089	1.5	0.682	1.102
F4	11.3	0.086	1.9	0.726	1.117
F5	14.0	0.084	2.6	0.723	1.174
F6	19.6	0.082	3.3	0.746	1.091
F7	9.9	0.152	3.0	0.514	0.849
F8	9.7	0.323	8.0	0.370	0.620
F9	10.0	0.74	21.7	0.243	0.473
F10	20.0	0.50	38.2	0.258	0.514
F11	10.0	2.08	50.0	0.228	0.418
F12	10.0	0.36	7.0	0.351	0.656
F13	10.8	0.088	1.6	0.691	1.136

Table 1: Characteristics of the tested grain size distribution curves: Fines content FC , mean grain size d_{50} , uniformity coefficient $C_u = d_{60}/d_{10}$ and minimum and maximum void ratios e_{\min} , e_{\max}

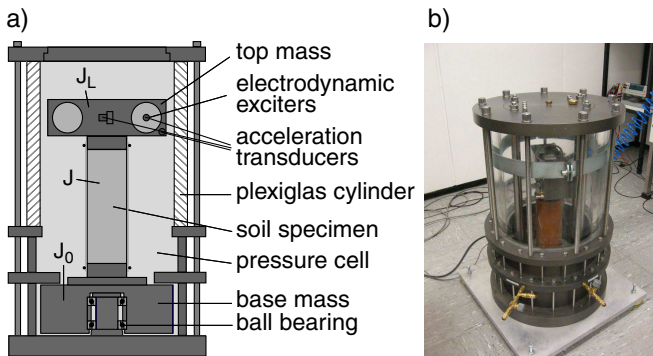


Fig. 4: Resonant Column device used for the present study: a) scheme and b) photo

generator, amplified and applied to the electrodynamic exciters. The frequency of excitation is varied until the resonant frequency f_R of the system composed of the two end masses and the specimen has been found. By definition, this is the case when $M(t)$ and $\theta(t)$ have a phase-shift of $\pi/2$ in time t . The secant shear modulus

$$G = \left(\frac{2\pi h f_R}{a} \right)^2 \varrho \quad (19)$$

is calculated from the resonant frequency, the height h and the density ϱ of the specimen. The parameter a is obtained from Eq. (20):

$$a \tan(a) - \frac{J^2}{J_0 J_L} \frac{\tan(a)}{a} = \frac{J}{J_0} + \frac{J}{J_L} \quad (20)$$

In Eq. (20) J is the polar moment of inertia of the specimen and $J_0 = 1.176 \text{ kg m}^2$ and $J_L = 0.0663 \text{ kg m}^2$ are the respective values of the base mass and the top mass (Fig. 4a). The polar moment of inertia of the top mass has been calibrated by means of aluminium rods with different diameters and known stiffnesses.

Different shear strain amplitudes can be tested by varying the amplitude of the torsional excitation. All tested specimens had a full cross section and measured $d = 10 \text{ cm}$ in diameter and $h = 20 \text{ cm}$ in height. The shear strain

amplitude is not constant within the sample volume, but depends on the distance x of a point from the bottom of the sample and on the radius r measured from the symmetry axis. Having measured the rotation angle θ_{\max} at the top of the sample at the time of maximum twist, the shear strain amplitude in a point (r, x) can be calculated from [24]

$$\gamma(r, x) = -r \frac{a}{h} \theta_{\max} \frac{\sin\left(\frac{ax}{h}\right) + \frac{J_0}{J} a \cos\left(\frac{ax}{h}\right)}{\cos(a) - \frac{J_0}{J} a \sin(a)} \quad (21)$$

A mean value of γ over the sample volume is used for the analysis of the tests:

$$\bar{\gamma} = \frac{1}{V} \int_V \gamma(r, x) dV \quad (22)$$

This mean value is simply denoted by γ in the following. Preliminary tests on hollow cylinder samples (outer diameter $d_a = 10 \text{ cm}$, inner diameter $d_i = 6 \text{ cm}$, $h = 10 \text{ cm}$), having a more uniform distribution of shear strains over the cross section, showed similar curves $G(\gamma)$ and $D(\gamma)$ as full cylinder specimens. The shear strain amplitudes that can be tested in the RC device lie in the range $5 \times 10^{-7} \leq \gamma \leq 5 \times 10^{-4}$.

For P-wave measurements the specimen end plates have been additionally equipped with piezoelectric elements. The transducers are similar to those explained by Brignoli et al. [6]. A single sinusoidal signal with a frequency of $f = 20 \text{ kHz}$ was applied to the element in the base pedestal. The travel time t_t has been determined from the first arrival of the signal received at the top cap. Typical signals have been presented in [26]. Delay times in cables, amplifiers, etc. have been subtracted from t_t . Based on the literature the strain amplitudes generated in the soil using this type of P-wave sensors are assumed to be less than 10^{-6} . In [30] it has been demonstrated that the G_{\max} -values obtained from S-wave velocity measurements by means of piezoelectric elements are close to the G_{\max} -values measured with the RC device.

The lateral deformations and the settlement of the samples were measured with non-contact displacement transducers.

All specimens were prepared by air pluviation and tested in the air-dry condition. In order to minimize segregation in case of the more well-graded mixtures (F7 - F12) the fall height of the sand during pluviation was chosen relatively small ($< 2 \text{ cm}$). Different densities were achieved by varying the outlet diameter of the funnel. Although other sample preparation methods like moist tamping would completely avoid segregation, the air pluviation technique was chosen also for the more well-graded silty sands in order to keep the test results comparable to the data already available for clean sands [25–29], where the samples were also prepared by air pluviation.

For each material several specimens with different initial relative densities D_{r0} were tested. The mean pressure p was increased step-wise from $p = 50$ to 400 kPa . At each pressure p the small strain shear modulus G_{\max} and the P-wave velocity v_P were measured after a resting period of 5 minutes, in order to obtain a similar "aging" (Affi & Woods [4], Affi & Richart [3], Baxter [5]) of the samples. Finally, the curves $G(\gamma)$ and $D(\gamma)$ were measured at $p = 400 \text{ kPa}$. In three additional tests on medium dense specimens the modulus degradation and the damping ratio were also measured at $p = 50, 100$ and 200 kPa for each material.

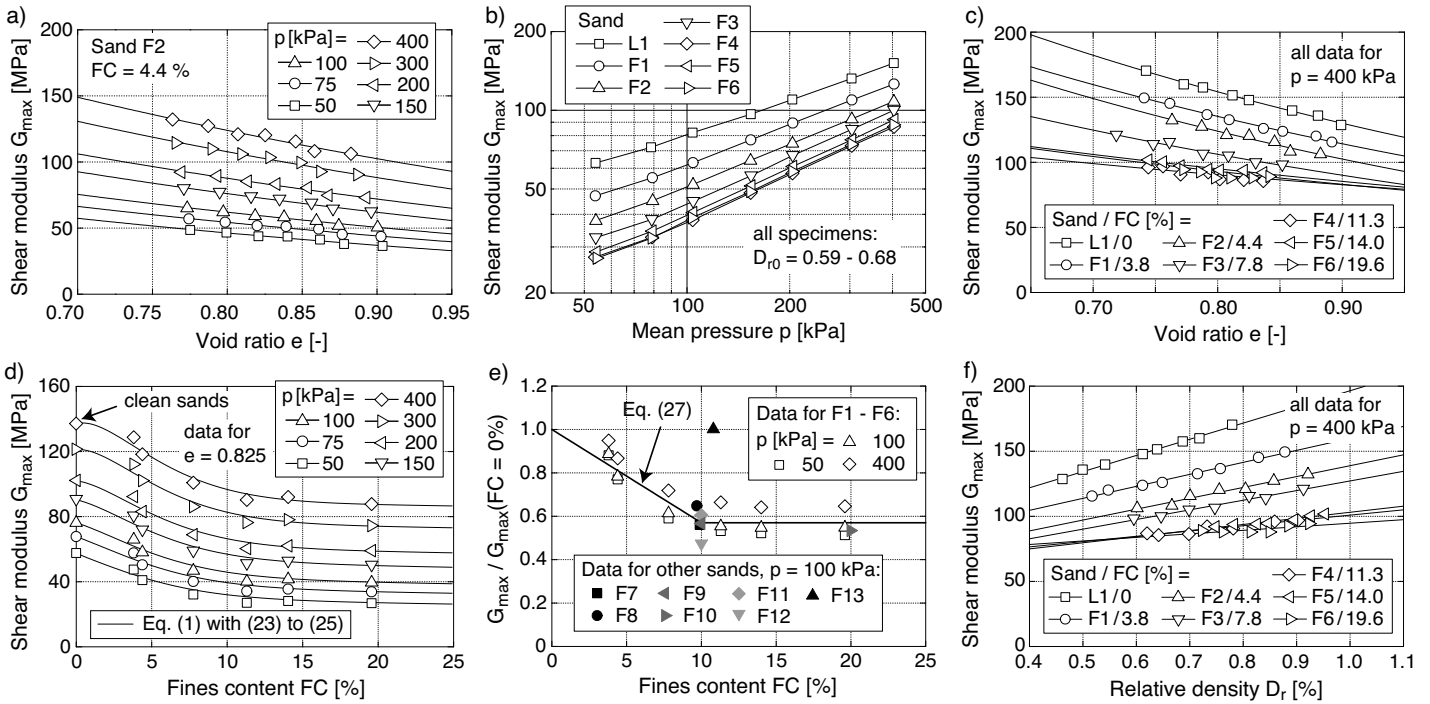


Fig. 5: a) Typical data of small strain shear modulus G_{\max} as a function of void ratio e and mean pressure p , b) G_{\max} versus p for medium dense specimens of sands F1 to F6, c) Comparison of $G_{\max}(e)$ for sands with different fines content, d) G_{\max} for $e = 0.825 = \text{constant}$ versus fines content FC, e) Ratio of $G_{\max}(FC)$ for silty sand and $G_{\max}(FC = 0\%)$ for clean sand versus FC, f) G_{\max} as a function of relative density D_r .

4 Small strain shear modulus G_{\max}

4.1 Poorly graded silty sands F1 to F6

Figure 5a presents G_{\max} as a function of void ratio e and mean pressure p exemplary for sand F2. The well-known increase of G_{\max} with decreasing void ratio and increasing pressure is obvious in Figure 5a. The linear curves of G_{\max} versus p in the double-logarithmic scale (Fig. 5b) confirm the power-law relationship $G_{\max} \sim p^n$.

The comparison of the curves $G_{\max}(e)$ for the clean sand L1 ($d_{50} = 0.1$ mm, $C_u = 1.5$, see grain size distribution curve in Figure 3, data taken from Wichtmann & Triantafyllidis [25]) and for the silty sands F1 to F6 in Fig. 5c reveals that for constant values of void ratio and pressure, the small-strain shear modulus G_{\max} significantly decreases with increasing fines content. No further noticeable reduction of G_{\max} was observed when FC was increased above approx. 10%. This becomes obvious also in Fig. 5d where G_{\max} for $e = 0.825 = \text{constant}$ is plotted versus the fines content.

The reduction of G_{\max} with increasing fines content can be quantified from the data in Fig. 5e. It shows the small-strain shear modulus of a silty sand divided by the G_{\max} -value of clean sand (calculated from Eqs. (1) to (4)) at same values of void ratio and pressure. On average, G_{\max} for $FC > 10\%$ amounts about 57% of the value for clean sand. The reduction of G_{\max} with increasing FC is somewhat larger for smaller pressures which is in good accordance with Salgado et al. [21] and Sahaphol & Miura [20] (see Figure 2).

Up to $FC = 10\%$ the reduction of G_{\max} with increasing fines content observed in the present study is similar to that reported by Salgado et al. [21] and somewhat smaller than that measured by Iwasaki & Tatsuoka [12] (Fig. 2). For a

fines content $FC > 10\%$ Iwasaki & Tatsuoka [12] and Salgado et al. [21] reported a further decrease of G_{\max} while almost constant values were obtained in the present study. The differences may be due to the fact that gap-graded mixtures were tested in the literature while continuous grain size distribution curves with fines have been examined in the present study. Compared to the relationship $G_{\max}(FC)$ obtained in the present study, the step-shaped function proposed by Randolph et al. [19] significantly overestimates the reduction of G_{\max} with FC (Fig. 2).

In contrast to clean sands with various d_{50} - and C_u -values, the small-strain shear modulus G_{\max} of silty sands cannot be described by a unique function of relative density D_r . Similar to the diagram with $e = \text{constant}$ (Fig. 5c), also for $D_r = \text{constant}$ G_{\max} strongly decreases with increasing fines content (Fig. 5f). Therefore, Eq. (5) cannot be generalized for silty sands.

4.2 Empirical formulas

Based on the data for sands F1 to F6, the correlations (2) to (4) have been extended by the influence of the fines content. The parameters A , a and n resulting from a curve-fitting of Eq. (1) to the $G_{\max}(e, p)$ data are plotted versus FC in Figure 6. The increase of a with FC reflects the flatter curves $G_{\max}(e)$ for higher FC-values (Fig. 5c). The increase of n with FC corresponds to steeper curves $G_{\max}(p)$ (Fig. 5b) for larger fines contents which is in good agreement with Salgado et al. [21]. The following extension of the correlations (2) to (4) has been derived based on the data in Fig. 6:

$$a = 1.94 \exp(-0.066 C_u) \exp(0.065 FC) \quad (23)$$

$$n = 0.40 C_u^{0.18} [1 + 0.116 \ln(1 + FC)] \quad (24)$$

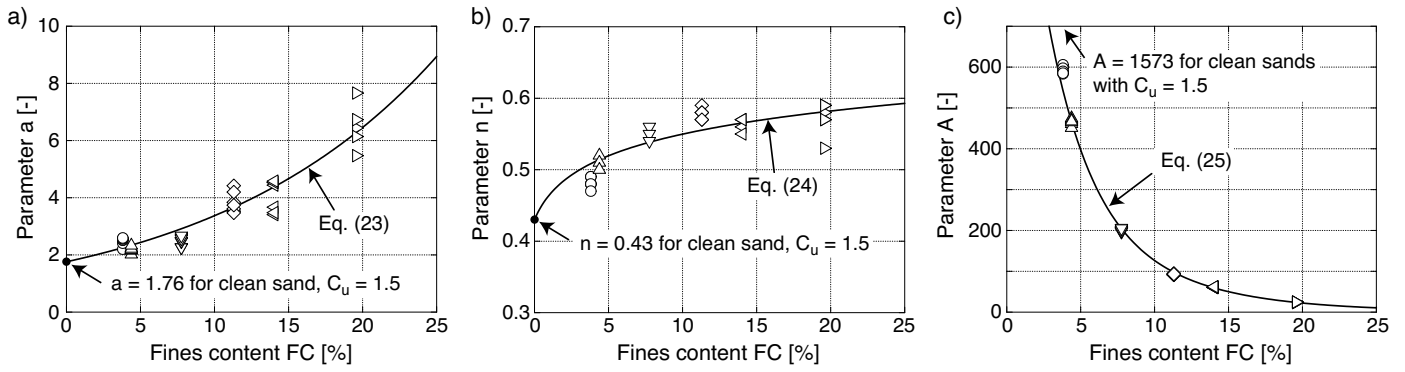


Fig. 6: Parameters A , a and n of Eq. (1) as a function of fines content FC . For each sand, the data is given for a) different pressures p and b),c) different relative densities D_{r0}

$$A = (1563 + 3.13 C_u^{2.98}) \cdot \frac{1}{2} \cdot [\exp(-0.30FC^{1.10}) + \exp(-0.28FC^{0.85})] \quad (25)$$

Only the sum of two exponential functions turned out to be flexible enough to approximate the $A(FC)$ data. For $FC = 0$, the equations for clean sands are regained from Eqs. (23) to (25).

Eq. (1) with the correlations (23) to (25) was used to generate the solid curves plotted in Fig. 5d. In Figure 7a the shear modulus G_{\max}^{pred} predicted by Eq. (1) with (23) to (25) is plotted versus the measured data G_{\max}^{meas} for all tested pressures and densities. Most of the data points plot close to the bisecting line described by $G_{\max}^{\text{pred}} = G_{\max}^{\text{meas}}$, confirming a good prediction quality.

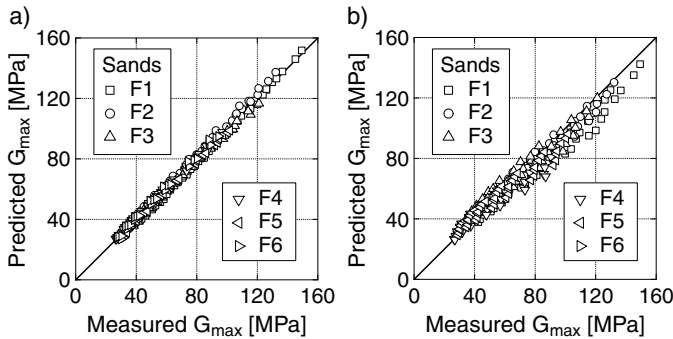


Fig. 7: G_{\max} -values predicted by a) Eq. (1) with (23) to (25) or b) Eqs. (26) and (27) versus measured G_{\max} -data

It has to be stressed that for sands with $FC > 10\%$ the correlations (23) to (25) should be evaluated with a C_u -value that corresponds to the average inclination $C_{u,d>0.063}^{\text{av}}$ (see Fig. 3a) of the grain size distribution curve in the range of grain sizes $d > 0.063$ mm (e.g. $C_u = 1.5$ for sands F4, F5 and F6).

Alternatively, G_{\max} of silty sand can be described by a multiplicative approach:

$$G_{\max}(FC) = G_{\max}(FC = 0) f_r(FC) \quad (26)$$

wherein $G_{\max}(FC = 0)$ is the small-strain shear modulus for clean sand, calculated e.g. from Eqs. (1) to (4), and $f_r(FC)$ is a reduction factor depending on fines content. A bilinear approach (solid line in Fig. 5e) is proposed:

$$f_r(FC) = \begin{cases} 1 - 0.043 FC & \text{for } FC \leq 10\% \\ 0.57 & \text{for } FC > 10\% \end{cases} \quad (27)$$

Mat.	Eq. (1) + (23)-(25)			Eqs. (26) + (27)		
	$\leq 10\%$	$< 20\%$	$< 30\%$	$\leq 10\%$	$< 20\%$	$< 30\%$
F1 - F6	99	100	100	71	99	100
F7 - F12	27	66	89	62	88	95

Table 2: Mean percentage values of predicted G_{\max} data differing $\leq 10\%$, $\leq 20\%$ or $\leq 30\%$ from the experimental data

Figure 7b presents the small-strain shear modulus predicted by Eqs. (1) to (4) with (26) to (27) plotted versus the measured data. The prediction is slightly less accurate than in the case of Eq. (1) with (23) to (25) (Fig. 7a). This becomes clear also from the first row of data in Table 2, where the mean percental values of predicted G_{\max} data differing $\leq 10\%$, $\leq 20\%$ or $\leq 30\%$ from the experimental data are given.

In the present study, according to German standard codes, the fines content was defined as the mass percentage of grains with size $d < 0.063$ mm. The question arises if the empirical equations developed in this paper can be also applied if $d < 0.074$ mm is used as the criterion for the fines, as in most studies in the literature. Looking at the schematic drawing in Figure 8, according to [25] two clean quartz sands with parallel grain size distribution curves A and B should have the same G_{\max} value since C_u is identical and d_{50} does not influence the small-strain stiffness. Based on those findings, it can be also expected that the G_{\max} -values of the silty sands C and D are similar (but lower than those of A and B), since their grain size distribution curves are parallel as well. The shape of the grain size distribution curves of sands C and D is similar to those of sands F1 to F6 tested in the present study. Sand C has 20% grains with $d < 0.063$ mm while sand D is composed of 20% grains with $d < 0.074$ mm. Similar data as that shown in Figure 5e (for sands of type C) would have been probably obtained if grain size distribution curves with a sharp bend at $d = 0.074$ mm (type D) were tested. Based on these considerations, it can be concluded that the empirical equations developed for fines content defined by $d < 0.063$ mm in this paper should deliver meaningful results as well if the fines content is defined by the criterion $d < 0.074$ mm.

4.3 Well graded silty sands

The small-strain shear modulus of more well-graded sands is also reduced by a fines content. This becomes clear from

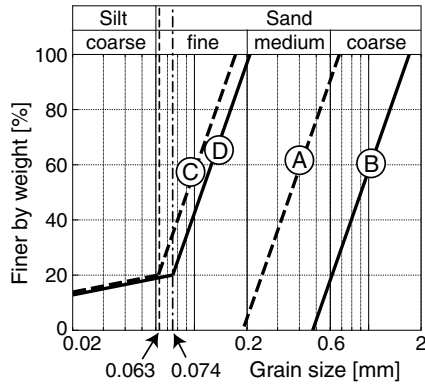


Fig. 8: Parallel grain size distribution curves with either 20 % grains with $d < 0.063$ mm (sand C) or 20 % grains with $d < 0.074$ mm (sand D)

Fig. 9 where the curves $G_{\max}(e)$ measured for the sands F7 and F8 with $C_u = 3$ or $C_u = 8$, respectively, are compared to the data (taken from [25]) obtained for clean sands with same uniformity coefficient. For a constant void ratio, the G_{\max} -value of silty sand is considerably lower than the small-strain shear modulus of clean sand.

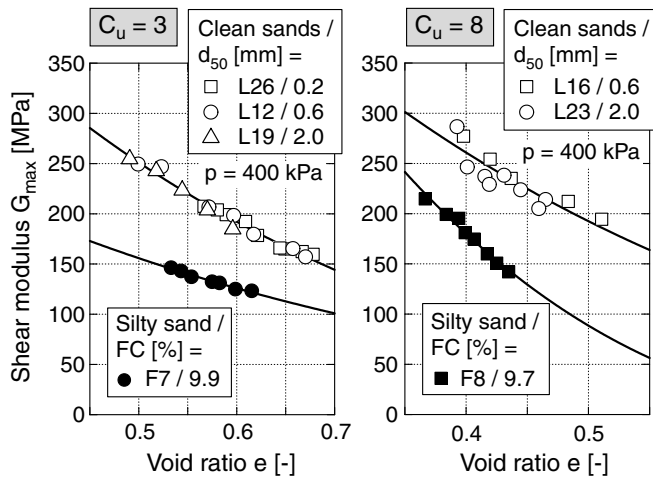


Fig. 9: Comparison of $G_{\max}(e, p)$ for clean sands and silty sands with uniformity coefficients $C_u = 3$ or 8 , respectively

The ratios $G_{\max}(FC)/G_{\max}(FC = 0)$ obtained for the more well-graded silty sands at $p = 100$ kPa have been also added in Figure 5e. The data for sands F7 to F11 agree well with those measured for the poorly graded sands F1 to F6, confirming that the G_{\max} degradation with increasing fines is rather independent of the uniformity coefficient. In case of the sand-gravel mixture F12, a somewhat larger decrease of G_{\max} than for F1 to F6 has been measured (Fig. 5e).

When calculating the value $G_{\max}(FC = 0)$ for F9, F10 and F12, the large uniformity coefficients $C_u = 21.7$, 38.2 and 50.0 imposed problems since these values lie outside the range $1.5 \leq C_u \leq 16$ for which the validity of Eqs. (1) to (4) has been proven. An application of Eqs. (2) to (4) to C_u -values as high as 50 delivers non-meaningful parameters, e.g. a -values around 0.15 which are smaller than the tested void ratios (usually a should be significantly larger than the range of void ratios typical for a sand). Since the decrease of G_{\max} with C_u tends to an asymptotic value at $C_u \approx 16$,

it has been decided to evaluate the $G_{\max}(FC = 0)$ values for F9, F10 and F12 with $C_u = 16$ entering the correlations (2) to (4). However, the $G_{\max}(FC)/G_{\max}(FC = 0)$ data for F9, F10 and F12 in Figure 5e are consequently associated with some uncertainty.

In the case of the well-graded silty sands F7 to F12 the prediction quality of Eq. (1) with the correlations (23) to (25) is rather poor (see second row of data in Table 2). This is due to the fact that the strong increase of the parameters a and n with FC observed for $C_u = 1.5$ (Figure 6a,b) is less pronounced for higher C_u -values. Therefore, the application of Eqs. (23) to (25) should be restricted to relatively low C_u -values. In order to consider the combined C_u - and FC -influence in Eqs. (23) to (25) more accurately, further tests with a variation of FC at higher C_u -values are necessary.

As demonstrated by the data in the second row of Table 2, the multiplicative approach defined by Eqs. (26) and (27) delivers a better prediction of the experimental data for sands F7 to F12. It is thus recommended for a practical application, in particular in the case of well-graded sands with fines content.

4.4 Influence of the grain size distribution curve at $d < 0.063$ mm

The G_{\max} -values measured for the sand F13, containing 10.8 % fines in the range of particle sizes $0.04 \leq d < 0.063$ mm only, are nearly the same as those obtained for clean sand. This becomes clear from the $G_{\max}(FC)/G_{\max}(FC = 0)$ data given for $p = 100$ kPa in Figure 5e. Therefore, the reduction of G_{\max} by a non-cohesive fines content depends strongly on the grain size distribution curve of the fines. The practical application of the empirical equations developed in this paper should be restricted to silty sands with a grain size distribution curve in the range $d < 0.063$ mm similar to the tested quartz powder (see Figure 3).

4.5 Micromechanical explanation

The decrease of small-strain stiffness with increasing fines content can be explained similarly to the decrease of G_{\max} caused by an increasing C_u (Wichtmann & Triantafyllidis [25]). Simulations of Radjai & Wolf [15] and Radjai et al. [16] have shown that strong and weak force chains are formed through the interparticle contacts in a polydisperse material representing a non-uniformly composed granular packing, while the force chains are rather equally distributed in a monodisperse material, i.e. a uniformly composed sand. The shear forces transmitted by the weak contacts are negligibly small. Thus, in a polydisperse packing a large portion of grains are only marginally involved in the transmission of external shear forces but decrease void ratio since they occupy space in the grain skeleton. Therefore, for a constant void ratio the overall shear stiffness of the polydisperse packing is lower than that of the monodisperse one. A larger amount of small grains (i.e. in the range of grain sizes $d < 0.063$ mm classified as fines content) renders the packing more polydisperse, thus reducing its stiffness.

Strictly speaking, the concept of "skeleton" or "equivalent" void ratio used by several researchers in the literature (e.g. [14, 17, 18, 23]) is applicable to binary packings only, i.e. mixtures of two granular materials with significantly different grain size. However, the concept may be useful in order to tentatively explain the test results obtained in

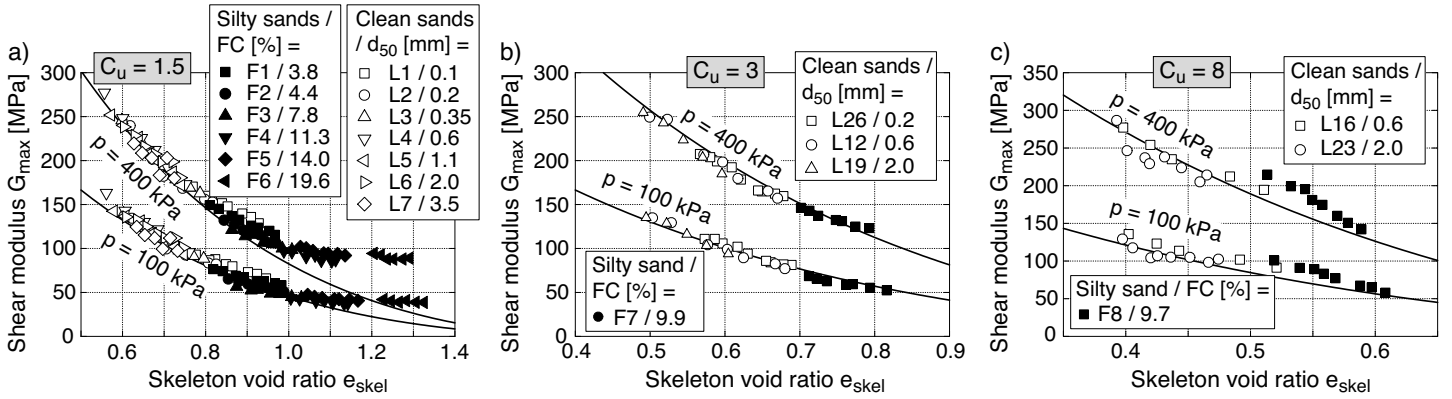


Fig. 10: Small-strain shear modulus G_{\max} of clean and silty sands versus skeleton void ratio $e_{\text{skel}} = (e + FC[\%]/100)/(1 - FC[\%]/100)$. For clean sands $e = e_{\text{skel}}$ holds. Solid curves = Prediction of Eqs. (1) to (4) with e_{skel} instead of e .

the present study. In a binary packing of large and small grains, below a "limiting fines content" the small grains primarily fill the voids between the large grains. Although they reduce the void ratio, the fine grains do not significantly influence the mechanical properties (e.g. G_{\max}) of the skeleton formed by the large grains. Consequently, considering same values of void ratio e , G_{\max} decreases with increasing fines content. The "skeleton void ratio", defined as the void ratio that would exist in the packing if all fine particles were removed, has been reported to be more representative for the sand behavior at small FC -values [14]. Some authors (e.g. [17,18,23]) consider that with increasing fines content, an increasing fraction of the fines also contributes to the force transfer in the soil. Although the silty sands tested in the present study consist of various sizes of grains, the effect of the smaller grains may be quite similar to the role of the fines in the binary packing.

The latter assumption has been tentatively checked by calculating the skeleton void ratio $e_{\text{skel}} = (e + FC[\%]/100)/(1 - FC[\%]/100)$ for the silty sands. Using this equation implies the simplified assumption, that no fines are active in load transfer, i.e. the fines do only occupy void space (more sophisticated equations considering a fraction of fines involved in load transfer have been proposed e.g. in [17,18,23]). Afterwards G_{\max} has been plotted versus e_{skel} in Figure 10. For a certain pressure, the data $G_{\max}(e_{\text{skel}})$ of the silty sands agree surprisingly well with the shear moduli for clean sands (where $e = e_{\text{skel}}$ applies) with identical uniformity coefficients (Figure 10). For void ratios $e \leq 1.0$ the data $G_{\max}(e_{\text{skel}})$ of the sands with fines can even be sufficiently well described by Eqs. (1) to (4) developed for clean sands, if Eq. (1) is applied with e_{skel} instead of e (see solid curves in Figure 10). The larger deviations between the experimental $G_{\max}(e_{\text{skel}})$ data and the prediction by Eqs. (1) to (4) in the range $e > 1.0$ may be primarily attributed to the fact that such large void ratios have not been studied in the tests on clean sands, i.e. they lie beyond the range of applicability of Eqs. (2) to (4). Furthermore, the equation $e_{\text{skel}} = (e + FC[\%]/100)/(1 - FC[\%]/100)$ gets inaccurate at higher values of FC . However, it should be kept in mind that the application of the skeleton or equivalent void ratio concept to silty sands with continuous gradings is questionable because the choice of a certain grain size (e.g. $d = 0.063$ mm or 0.074 mm) separating the fine from the coarse particles is rather arbitrary. Therefore, it cannot be recom-

Mat.	Eq. (6) + (28)-(30)			Eqs. (31) + (32)		
	$\leq 10\%$	$\leq 20\%$	$\leq 30\%$	$\leq 10\%$	$\leq 20\%$	$\leq 30\%$
F1 - F6	99	100	100	59	89	100
F7 - F12	19	63	91	78	94	97

Table 3: Mean percentage values of predicted M_{\max} data differing $\leq 10\%$, $\leq 20\%$ or $\leq 30\%$ from the experimental data

mended to estimate the small-strain stiffness of silty sands with continuous gradings by applying Eqs. (1) to (4) with e_{skel} instead of e .

5 Constrained elastic modulus M_{\max}

5.1 Poorly graded silty sands F1 to F6

The decrease of the constrained elastic modulus M_{\max} with increasing fines content is apparent from the comparison of the $M_{\max}(e)$ curves in Figure 11a, from the M_{\max} - FC relationship given for a constant void ratio $e = 0.825$ in Figure 11b and from the $M_{\max}(FC)/M_{\max}(FC = 0)$ plot in Figure 11c. The diagrams in Figure 11b,c show that similar to G_{\max} the small-strain constrained elastic modulus stays almost constant if the fines content exceeds 10%. The analysis of the $M_{\max}(D_r)$ data showed that Eq. (10) cannot be generalized for silty sands.

5.2 Empirical equations

A similar set of equations as developed for G_{\max} has been established for M_{\max} . Based on a curve-fitting of Eq. (6) to the $M_{\max}(e, p)$ data of sands F1 to F6, the correlations (7) to (9) have been extended by the influence of the fines content:

$$a = 2.16 \exp(-0.055 C_u) (1 + 0.116 FC) \quad (28)$$

$$n = 0.344 C_u^{0.126} [1 + 0.125 \ln(1 + FC)] \quad (29)$$

$$A = (3655 + 26.7 C_u^{2.42}) \cdot \frac{1}{2} \cdot [\exp(-0.42FC^{1.10}) + \exp(-0.52FC^{0.60})] \quad (30)$$

The quite good approximation of the experimental data for F1 to F6 by Eq. (6) with (28) to (30) is demonstrated by the solid curves in Figure 11b and by the first row of data in Table 3, where the mean percentage values of predicted M_{\max} data differing $\leq 10\%$, $\leq 20\%$ or $\leq 30\%$ from the experimental data are given.

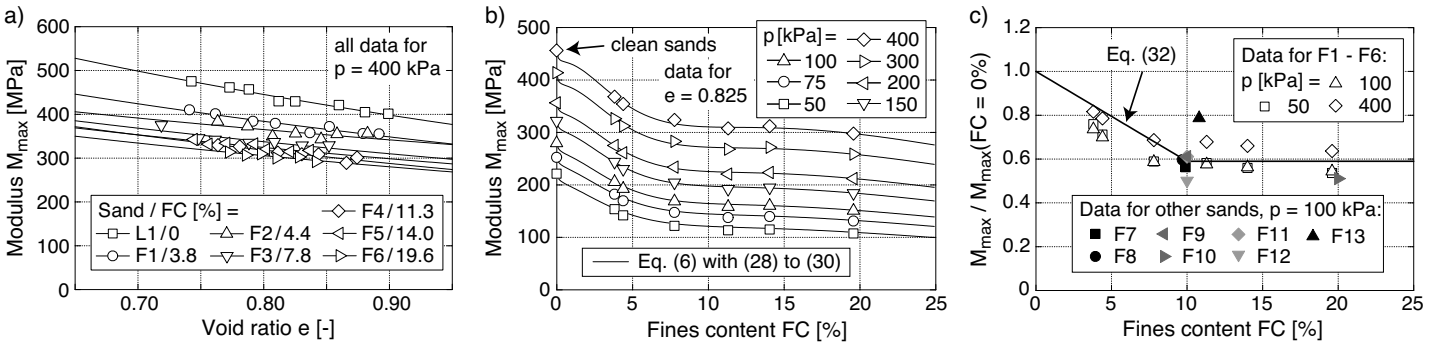


Fig. 11: a) Comparison of $M_{max}(e)$ for sands with different fines content (L1 data taken from [26]), b) M_{max} for $e = 0.825 = \text{constant}$ versus fines content FC , c) Ratio of $M_{max}(FC)$ for silty sand and $M_{max}(FC = 0\%)$ for clean sand versus FC

Alternatively, based on the data in Figure 11c a multiplicative approach has been also developed (see the solid line in Figure 11c):

$$M_{max}(FC) = M_{max}(FC = 0) f_r(FC) \quad \text{with (31)}$$

$$f_r(FC) = \begin{cases} 1 - 0.041 FC & \text{for } FC \leq 10 \% \\ 0.59 & \text{for } FC > 10 \% \end{cases} \quad (32)$$

The first row of data in Table 3 reveals that the prediction by Eqs. (31) and (32) is less accurate than that of Eq. (6) with (28) to (30).

5.3 Well graded silty sands

M_{max} decreases with fines content also for the more well-graded sands F7 and F8 (Figure 12). The percentage decrease is similar for all tested silty sands F1 to F12, independent of the uniformity coefficient (Figure 11c). The experimental data for the well-graded silty sands F7 to F12 is better approximated by the bilinear approach established by Eqs. (31) and (32) than by Eq. (6) with (28) to (30) (see second row of Table 3).

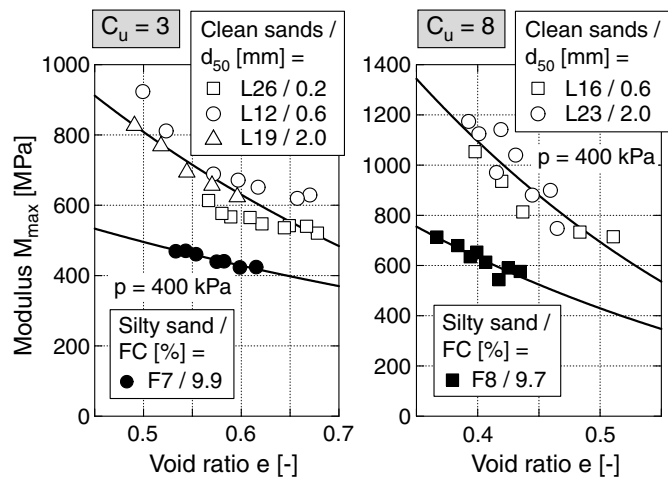


Fig. 12: Comparison of $M_{max}(e, p)$ for clean and silty sands with uniformity coefficients $C_u = 3$ or 8

5.4 Influence of the grain size distribution curve at $d < 0.063$ mm

The M_{max} values of sand F13 are lower than those for clean sand, but the $M_{max}(FC)/M_{max}(FC = 0)$ data are higher

than those obtained for the other tested silty sands (Figure 11c). As expected also the constrained elastic modulus of silty sand depends on the grain size distribution at $d < 0.063$ mm.

5.5 Poisson's ratio

Eq. (1) with the correlations (23) to (25) for G_{max} and Eq. (6) with the correlations (28) to (30) for M_{max} can be used to calculate Poisson's ratio ν for sands F1 to F6. In Figure 13, ν predicted for a constant void ratio $e = 0.825$ and different pressures is given as a function of the fines content FC . Poisson's ratio slightly decreases with increasing pressure. The variation of ν with fines content can be neglected for practical purposes.

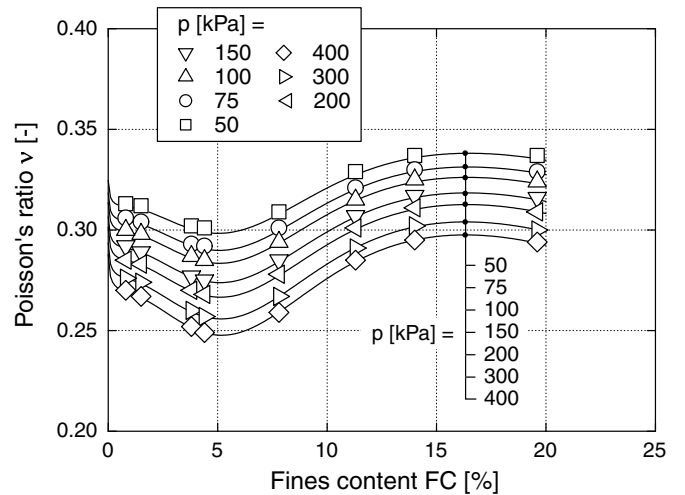


Fig. 13: Poisson's ratio ν for a constant void ratio $e = 0.825$ as a function of fines content FC , calculated from Eq. (1) with the correlations (23) to (25) and from Eq. (6) with the correlations (28) to (30)

A similar increase of Poisson's ratio with increasing uniformity coefficient as observed for clean sands [26] has been measured also for the silty sands F1 to F12. While the mean value of Poisson's ratio is $\nu = 0.29$ for the uniform silty sands F1 to F6, the respective values are $\nu = 0.31, 0.33, 0.36, 0.38, 0.35$ and 0.36 for sands F7, F8, F9, F10, F11 and F12.

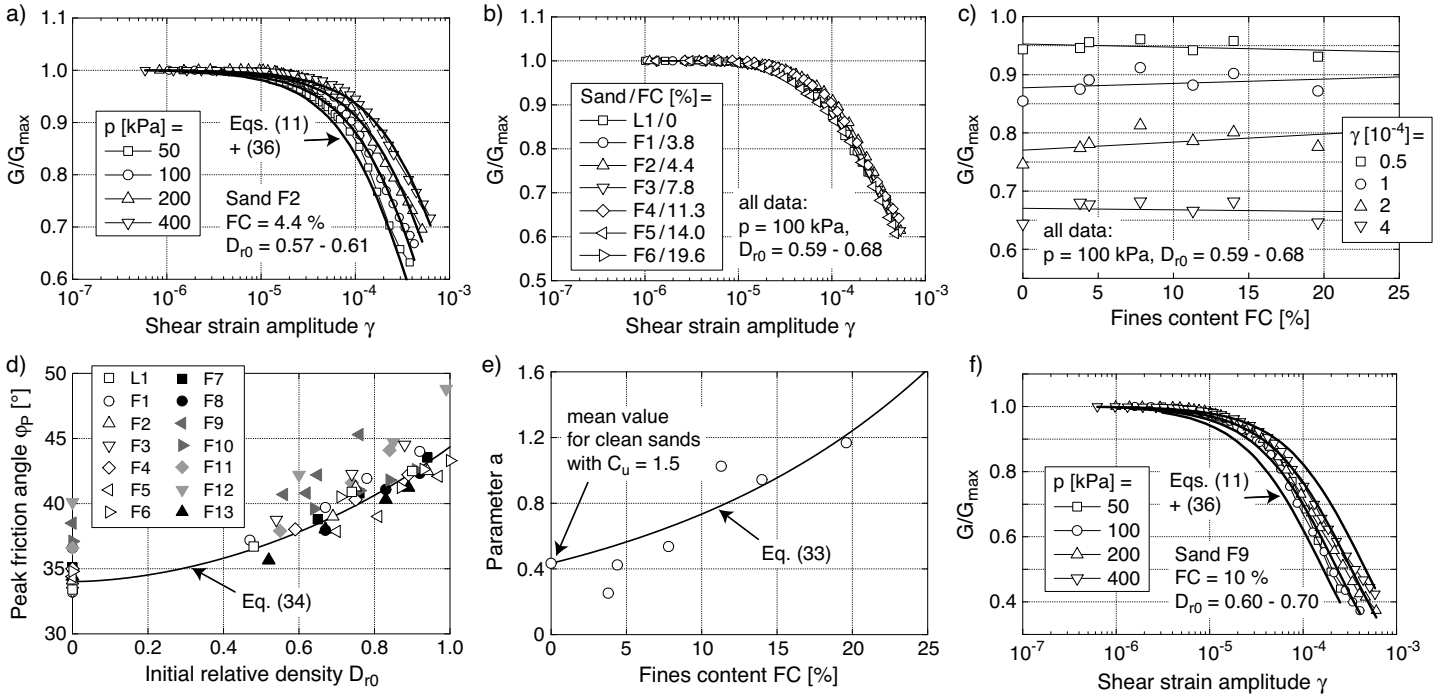


Fig. 14: a) Modulus degradation curves $G(\gamma)/G_{\max}$ measured for sand F2 at different pressures, b) Comparison of modulus degradation curves $G(\gamma)/G_{\max}$ for sands with different fines content, c) Factor G/G_{\max} for certain shear strain amplitudes γ as a function of fines content FC , d) Peak friction angle φ_P from drained monotonic triaxial tests as a function of initial relative density D_{r0} , e) Parameter a in Eq. (11) versus fines content, f) Modulus degradation curves $G(\gamma)/G_{\max}$ measured for material F9

6 Modulus degradation curves $G(\gamma)/G_{\max}$

6.1 Poorly graded silty sands F1 to F6

Modulus degradation curves $G(\gamma)/G_{\max}$ for different pressures are presented exemplary for sand F2 in Figure 14a. Similar to clean sands [13, 27], for a certain shear strain amplitude γ , the ratio G/G_{\max} increases with increasing pressure p . In contrast, the modulus degradation curves are almost independent of soil density.

No significant influence of fines content on the modulus degradation curves could be detected. This is obvious in Figure 14b, where the curves $G(\gamma)/G_{\max}$ measured for medium dense samples of the materials F1 to F6 are compared. The data is provided for $p = 100$ kPa but looks similar for other pressures. The FC -independence of modulus degradation is confirmed also by Figure 14c, where G/G_{\max} for certain values of the shear strain amplitude γ is plotted versus FC .

For all tested materials, the modulus degradation curves for different pressures and densities fall together, if the shear strain amplitude γ is normalized either by the reference shear strain γ_r or by $\sqrt{p/p_{\text{atm}}}$, respectively. The reference shear strain $\gamma_r = \tau_{\max}/G_{\max}$ was calculated with the measured G_{\max} and with shear strength $\tau_{\max} = p \sin \varphi_P$. For each material the density-dependent peak friction angle φ_P was determined from drained triaxial compression tests (Fig. 14d).

6.2 Empirical equations

Eq. (11) with $b = 1$ has been fitted to the $G(\gamma/\gamma_r)/G_{\max}$ data of the sands F1 to F6. In Figure 14e, the resulting curve-fitting parameters a are plotted versus fines content. Although the curves $G(\gamma)/G_{\max}$ are rather independent of fines content (Fig. 14b), the parameter a of Eq. (11) in-

creases with FC due to the decrease of G_{\max} and hence the increase of γ_r with FC . Therefore, an extension of Eq. (12) considering the influence of fines content is necessary (see solid curve in Fig. 14e):

$$a = 1.070 \ln(C_u) \exp(0.053 FC) \quad (33)$$

The shear strength τ_{\max} necessary for the reference shear strain $\gamma_r = \tau_{\max}/G_{\max}$ used in Eq. (11) can be estimated with the peak friction angle φ_P from

$$\varphi_P = 34.0^\circ \exp(0.27 D_{r0}^{1.8}) \quad (34)$$

Eq. (34) developed for clean sand [27] is applicable also to silty sands (Figure 14d).

The extension of Eqs. (14) and (15) by fines content FC reads:

$$a = [1 + 0.847 \ln(C_u)] \exp(0.0205 FC) \quad (35)$$

$$a = [1093.7 + 1955.3 \ln(C_u)] \exp(-0.31 FC^{0.1}) \quad (36)$$

In case of Stokoe's Eqs. (16) and (17), the parameters $\alpha = 1.03$ and $k = 0.4$ derived for clean sands [27] were found applicable also for the tested silty sands F1 to F6. A factor considering fines content has to be added to Eq. (18):

$$\gamma_{r1} = 6.52 \cdot 10^{-4} \exp[-0.59 \ln(C_u)] \exp(0.33 FC^{0.1}) \quad (37)$$

A good prediction quality of the extended empirical equations can be concluded from Figure 14a, from the diagrams in Figure 15 and from the first row of data in Table 4. In Figure 14a the $G(\gamma)/G_{\max}$ curves predicted by Eq. (11) using $\sqrt{p/p_{\text{atm}}}$ instead of γ_r as a reference quantity, with $b = 1$ and a from Eq. (36) agree well with the measured data.

In Figure 15 the G/G_{\max} -data predicted by Eq. (11) with $b = 1$ and a from Eq. (33) (diagram on the left-hand side) and by Eq. (11) with $\sqrt{p/p_{\text{atm}}}$ instead of γ_r , $b = 1$ and a from Eq. (36) (diagram on the right-hand side) are plotted versus the experimental data. Most data points plot close to the bisecting line, confirming a good prediction quality. In Table 4 the percentage values of predicted G/G_{\max} data differing either ≤ 0.05 or ≤ 0.1 from the measured G/G_{\max} data are provided. Judging by the data in Table 4, the prediction quality of the different sets of equations for F1 to F6 is quite similar.

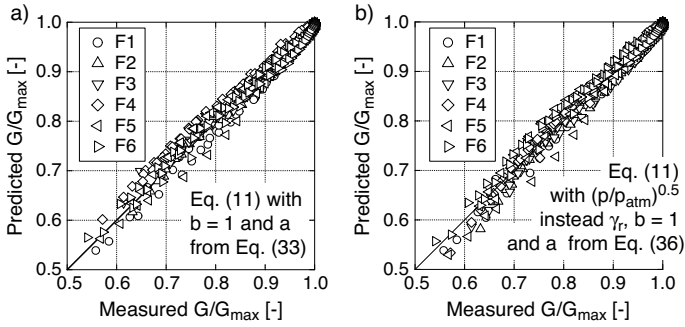


Fig. 15: Comparison of measured G/G_{\max} -data with the prediction by a) Eq. (11) with $b = 1$ and a from Eq. (33) and b) Eq. (11) with $\sqrt{p/p_{\text{atm}}}$ instead of γ_r , $b = 1$ and a from Eq. (36)

6.3 Well graded silty sands

For silty sands with a similar fines content, the modulus degradation is stronger for higher values of the uniformity coefficient. This becomes clear from the comparison of the $G(\gamma)/G_{\max}$ data for material F9 ($C_u = 21.7$) in Figure 15f ($G/G_{\max} \approx 0.7$ for $p = 100$ kPa and $\gamma = 10^{-4}$) and for sands F1 to F6 in Figure 15b ($G/G_{\max} \approx 0.9$ for $\gamma = 10^{-4}$). It is in good accordance with observations for clean sand [27]. The pressure-dependence of modulus degradation is somewhat weaker for the well-graded materials (compare Figure 15a and 15f).

The prediction quality of the various empirical equations discussed in Section 6.2 for well-graded silty sands is less than in case of the poorly-graded sands F1 to F6 (see the second row of data in Table 4). The best approximation of the experiments can be achieved by Eqs. (13) and (35), the worst one is obtained from Eqs. (11) and (33). Due to uncertainties in the estimation of γ_r (see scatter of φ_P data in Figure 14d) and considering the simplicity of the equations formulated in terms of $\sqrt{p/p_{\text{atm}}}$ it is recommended to use Eqs. (11) and (13) with $\sqrt{p/p_{\text{atm}}}$ instead of γ_r and with the correlation (36) for a practical application.

7 Damping ratio

For the sands with large fines content ($FC \geq 10\%$) and for low pressures ($p = 50$ kPa) significantly lower damping ratios were measured than for clean sands (up to factor 6). For larger pressures ($p = 400$ kPa) the differences in the damping ratio of clean and silty sands with $FC \geq 10\%$ are less pronounced (approx. factor 1.5). Based on the test results the damping ratio of clean sand $D(FC = 0)$ (see equations in [27]) can be reduced by a factor depending on

fines content and pressure:

$$D(FC) = D(FC = 0) f_{r,D} \quad (38)$$

$$f_{r,D} = \begin{cases} 1 - (1 - k) \frac{FC}{10\%} & \text{for } FC \leq 10\% \\ k & \text{for } FC > 10\% \end{cases} \quad (39)$$

with

$$k = \frac{1}{\exp[4.60 - 0.71 \ln(p)]} \quad (40)$$

8 Threshold amplitudes

The threshold shear strain amplitudes, indicating the transition from the linear elastic to the nonlinear elastic behaviour ($\gamma_{tl} = \gamma(G/G_{\max} = 0.99)$) or the onset of settlement (γ_{tv}) are plotted versus fines content in Figure 16. The given γ_{tl} - and γ_{tv} -values are mean values from the four tests with different pressures performed on medium dense samples. For a constant uniformity coefficient ($C_u = 1.5$, sands F1 - F6), both threshold values slightly increase with fines content (filled symbols in Figure 16). The silty sands with higher uniformity coefficients show lower γ_{tl} - and γ_{tv} -values than the poorly-graded silty sands (open symbols in Figure 16). A similar decrease of γ_{tl} with increasing C_u was also observed for clean sands [27].

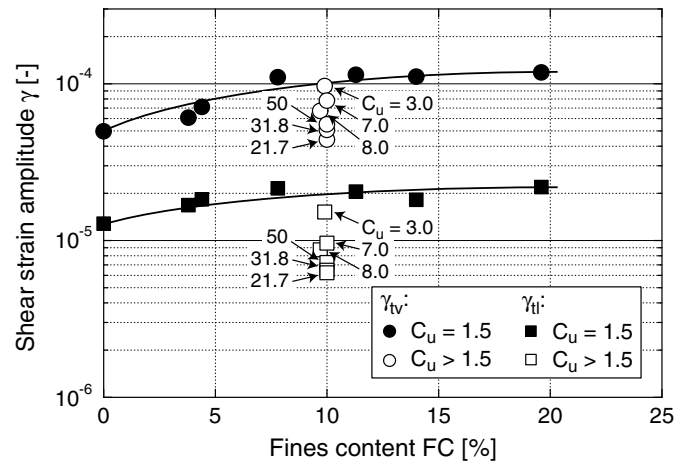


Fig. 16: Threshold shear strain amplitudes γ_{tl} and γ_{tv} versus fines content

9 Summary and conclusions

The influence of a non-cohesive fines content on small-strain shear modulus G_{\max} , small-strain constrained elastic modulus M_{\max} , shear modulus degradation $G(\gamma)/G_{\max}$, damping ratio $D(\gamma)$ and threshold shear strain amplitudes γ_{tl} and γ_{tv} has been studied in approx. 130 resonant column (RC) tests with P-wave measurements. Specially mixed continuous grain size distribution curves of a quartz sand with varying fines contents ($0 \leq FC \leq 20\%$, defined as the mass percentage of grains with size $d < 0.063$ mm according to DIN standard code) and uniformity coefficients ($1.5 \leq C_u \leq 50$) have been tested. For each material several specimens prepared with different relative densities were tested at various isotropic pressures.

The test results show that for constant values of void ratio and pressure both, G_{\max} and M_{\max} significantly decrease with increasing fines content. On average, G_{\max} and

Sand	Eq. (11) with $b = 1$				Eq. (13)				Eqs. (16), (17)	
	γ_r , Eq. (33)		$\sqrt{p/p_{atm}}$, Eq. (36)		γ_r , Eq. (35)		$\sqrt{p/p_{atm}}$, Eq. (36)		+ (37)	
	≤ 0.05	≤ 0.1	≤ 0.05	≤ 0.1	≤ 0.05	≤ 0.1	≤ 0.05	≤ 0.1	≤ 0.05	≤ 0.1
F1 - F6	99	100	98	100	97	100	98	100	98	100
F7 - F12	31	74	68	96	80	98	68	96	77	94

Table 4: Percentage of predicted G/G_{max} data differing ≤ 0.05 or ≤ 0.1 from measured G/G_{max} data. Only data with $G/G_{max} < 0.9$ is considered.

M_{max} of a silty sand with 10 % fines amount about 60 % of the respective values for clean sand. At $FC > 10$ % G_{max} and M_{max} remained almost constant if the fines content was further increased. The percental decrease of G_{max} and M_{max} with FC is nearly independent of the uniformity coefficient C_u .

An extension of empirical formulas for G_{max} and M_{max} considering the influence of fines content has been proposed. The application of the first approach, using C_u - and FC -dependent parameters of Hardin's equation should be restricted to poorly graded silty sands. The second approach, in which the small-strain stiffness evaluated for clean sand is reduced by a FC -dependent factor, is less accurate but applicable also to well-graded silty sands and thus recommended for a practical application.

At same values of FC , a material having fines only in the range of particle sizes $0.04 \leq d \leq 0.063$ mm showed considerably larger G_{max} and M_{max} -values than the silty sands containing a significant amount of grains with $d < 0.04$ mm. Therefore, the small-strain stiffness significantly depends on the grain size distribution curve of the non-cohesive fines. The application of the empirical equations proposed in this paper should be thus restricted to fines having a similar grain size distribution curve as the tested quartz powder.

The measured modulus degradation curves $G(\gamma)/G_{max}$ are almost independent of fines content. Empirical equations for modulus degradation developed for clean sands had to be extended by the influence of fines, however, since G_{max} and hence the reference shear strain γ_r decreases with FC .

A significant decrease of damping ratio with fines content was observed at low pressures (e.g. $p = 50$ kPa). It is less pronounced at higher pressures (e.g. $p = 400$ kPa). A reduction factor for the damping ratio considering the influence of a fines content has been proposed.

A slight increase of the threshold shear strain amplitudes $\gamma_{tl} = \gamma(G/G_{max} = 0.99)$ and γ_{tv} , indicating the transition from the linear elastic to the nonlinear elastic behaviour or the onset of settlement, respectively, with increasing fines content has been measured. In contrast, γ_{tl} and γ_{tv} decrease with increasing uniformity coefficient of the silty sand.

Acknowledgements

The presented study has been funded by the German Research Council (DFG, project Nos. TR218/11-1 and TR 218/17-1). The authors are grateful to DFG for the financial support. Parts of the laboratory tests have been performed during the former work of the authors at Ruhr-University Bochum, Germany.

References

- [1] DIN 18126: *Bestimmung der Dichte nichtbindiger Böden bei lockerster und dichtester Lagerung*, 1996.
- [2] DIN 18196: *Erd- und Grundbau Bodenklassifikation für bautechnische Zwecke*, 2006.
- [3] S.S. Afifi and Jr. Richart, F.E. Stress-history effects on shear modulus of soils. *Soils and Foundations*, 13(1):77–95, 1973.
- [4] S.S. Afifi and R.D. Woods. Long-term pressure effects on shear modulus of soils. *Journal of the Soil Mechanics and Foundations Division, ASCE*, 97(SM10):1445–1460, 1971.
- [5] C.D.P. Baxter. *An experimental study on the aging of sands*. PhD thesis, Faculty of the Virginia Polytechnic Institute and State University, July 1999.
- [6] G.M. Brignoli, M. Gotti, and K.H. II. Stokoe. Measurement of shear waves in laboratory specimens by means of piezoelectric transducers. *Geotechnical Testing Journal, ASTM*, 19(4):384–397, 1996.
- [7] G. Gazetas. *Foundation Engineering Handbook, 2nd Edition*, chapter 15: Foundation vibrations, pages 553–593. 1991.
- [8] B.O. Hardin and W.L. Black. Sand stiffness under various triaxial stresses. *Journal of the Soil Mechanics and Foundations Division, ASCE*, 92(SM2):27–42, 1966.
- [9] B.O. Hardin and V.P. Drnevich. Shear modulus and damping in soils: design equations and curves. *Journal of the Soil Mechanics and Foundations Division, ASCE*, 98(SM7):667–692, 1972.
- [10] B.O. Hardin and M.E. Kalinski. Estimating the shear modulus of gravelly soils. *Journal of Geotechnical and Geoenvironmental Engineering, ASCE*, 131(7):867–875, 2005.
- [11] B.O. Hardin and F.E. Richart Jr. Elastic wave velocities in granular soils. *Journal of the Soil Mechanics and Foundations Division, ASCE*, 89(SM1):33–65, 1963.
- [12] T. Iwasaki and F. Tatsuoka. Effects of grain size and grading on dynamic shear moduli of sands. *Soils and Foundations*, 17(3):19–35, 1977.
- [13] T. Kokusho. Cyclic triaxial test of dynamic soil properties for wide strain range. *Soils and Foundations*, 20(2):45–59, 1980.
- [14] C. Polito and J. Martin. Effects of nonplastic fines on the liquefaction resistance of sands. *Journal of Geotechnical and Geoenvironmental Engineering, ASCE*, 127(5):408–415, 2001.
- [15] F. Radjai and D.E. Wolf. Features of static pressure in dense granular media. *Granular Matter*, (1):3–8, 1998.
- [16] F. Radjai, D.E. Wolf, M. Jean, and J.-J. Moreau. Bimodal character of stress transmission in granular packings. *Physical Review Lett.*, 80(1):61–64, 1998.
- [17] M.M. Rahman and S.R. Lo. Predicting the onset of static liquefaction of loose sand with fines. *Journal of Geotechnical and Geoenvironmental Engineering, ASCE*, 138:1037–1041, 2012.

- [18] M.M. Rahman, S.R. Lo, and C.T. Gnanendran. On equivalent granular void ratio and steady state behaviour of loose sands with fines. *Canadian Geotechnical Journal*, 45(10):1439–1456, 2008.
- [19] M.F. Randolph, J. Dolwin, and R. Beck. Design of driven piles in sand. *Géotechnique*, 44(3):427–448, 1994.
- [20] T. Sahaphol and S. Miura. Shear moduli of volcanic soils. *Soil Dynamics and Earthquake Engineering*, 25:157–165, 2005.
- [21] R. Salgado, P. Bandini, and A. Karim. Shear strength and stiffness of silty sand. *Journal of Geotechnical and Geoenvironmental Engineering, ASCE*, 126(5):451–462, 2000.
- [22] K.H. Stokoe, M.B. Darendeli, R.D. Andrus, and L.T. Brown. Dynamic soil properties: laboratory, field and correlation studies. In *Proc. 2nd Int. Conf. on Earthquake Geotech. Eng.*, volume 3, pages 811–845. A.A. Balkema, 1999.
- [23] S. Thevanayagam. Effect of fines and confining stress on undrained shear strength of silty sands. *Journal of Geotechnical and Geoenvironmental Engineering, ASCE*, 124(6):479–491, 1998.
- [24] T. Wichtmann, T. Sonntag, and T. Triantafyllidis. Über das Erinnerungsvermögen von Sand unter zyklischer Belastung. *Bautechnik*, 78(12):852–865, 2001.
- [25] T. Wichtmann and T. Triantafyllidis. On the influence of the grain size distribution curve of quartz sand on the small strain shear modulus G_{\max} . *Journal of Geotechnical and Geoenvironmental Engineering, ASCE*, 135(10):1404–1418, 2009.
- [26] T. Wichtmann and T. Triantafyllidis. On the influence of the grain size distribution curve on P-wave velocity, constrained elastic modulus M_{\max} and Poisson's ratio of quartz sands. *Soil Dynamics and Earthquake Engineering*, 30(8):757–766, 2010.
- [27] T. Wichtmann and T. Triantafyllidis. Effect of uniformity coefficient on G/G_{\max} and damping ratio of uniform to well graded quartz sands. *Journal of Geotechnical and Geoenvironmental Engineering, ASCE*, 139(1):59–72, 2013.
- [28] T. Wichtmann and T. Triantafyllidis. Small-strain constrained elastic modulus M_{\max} of clean quartz sand with various grain size distribution curves. *Soil Dynamics and Earthquake Engineering*, 55(12):130–139, 2013.
- [29] T. Wichtmann and T. Triantafyllidis. Stiffness and damping of clean quartz sand with various grain size distribution curves. *Journal of Geotechnical and Geoenvironmental Engineering*, 140(3), 2014.
- [30] T. Wichtmann and Th. Triantafyllidis. Influence of a cyclic and dynamic loading history on dynamic properties of dry sand, part II: cyclic axial preloading. *Soil Dynamics and Earthquake Engineering*, 24(11):789–803, 2004.
- [31] P. Yu and F.E. Richart Jr. Stress ratio effects on shear modulus of dry sands. *Journal of Geotechnical Engineering, ASCE*, 110(3):331–345, 1984.